Flexible Control of Motor Units: Is the Multidimensionality of Motor Unit Manifolds a Sufficient Condition?

François DERNONCOURT[1], Simon AVRILLON[1,2], Tijn LOGTENS[1],
Thomas CATTAGNI[3], Dario FARINA[2] and François HUG[1,4]*

[1] Université Côte d'Azur, LAMHESS, Nice, France.
[2] Department of Bioengineering, Faculty of Engineering, Imperial College London, London, United Kingdom.
[3] Nantes Université, Laboratory "Movement, Interactions, Performance" (UR 4334), Nantes, France
[4] The University of Queensland, School of Biomedical Sciences, Brisbane, QLD, Australia

* Corresponding author
Prof. François Hug
Université Côte d'Azur, LAMHESS, Nice, France
Francois.hug@univ-cotedazur.fr

Running title: Control and dimensionality of motor unit manifolds

Supplemental data availability: The entire dataset (raw and processed data) and codes will be made available upon publication.

Conflict of interests: The authors declare no competing financial interests.

Funding resources: This study was funded by a grant from the French National Research Agency (ANR-24-CE17-5805; Neuromotor project). François Hug is supported by the French government, through the UCAJEDI Investments in the Future project managed by the ANR with the reference number ANR-15-IDEX-01 Dario Farina is supported by the European Research Council Synergy Grant NaturalBionicS (contract #810346), the EPSRC Transformative Healthcare, NISNEM Technology (EP/T020970), and the BBSRC, "Neural Commands for Fast Movements in the Primate Motor System" (NU-003743). The authors are grateful to the Université Côte d'Azur's Center for High-Performance Computing (OPAL infrastructure) for providing resources and support.

Author Contributions: Contribution and design of the experiment: FD, SA, FH; Collection of data: FD; Analysis and interpretation: FD, SA, TL, TC, DF, FH; Drafting the article or revising it for important intellectual content: FD, SA, TL, TC, DF, FH; All authors approved the final version of the manuscript.

Abstract

The level of flexibility in the neural control of motor units remains a topic of debate. Understanding this flexibility would require the identification of the distribution of common inputs to the motor units. In this study, we identified large samples of motor units from two lower limb muscles: the vastus lateralis (VL; up to 60 motor units/participant) and gastrocnemius medialis (GM; up to 67 motor units/participant). First, we applied a linear dimensionality reduction method to assess the dimensionality of the manifolds underlying the motor unit activity. We subsequently investigated the flexibility in motor unit control under two conditions: sinusoidal contractions with torque feedback, and online control with visual feedback on motor unit firing rates. Overall, we found that the activity of GM motor units was effectively captured by a single latent factor defining a unidimensional manifold, whereas the VL motor units were better represented by three latent factors defining a multidimensional manifold. Despite this difference in dimensionality, the recruitment of motor units in the two muscles exhibited similar but limited levels of flexibility. Using a spiking network model, we proposed that VL motor unit behaviors can be explained by a combination of a single common input of cortical origin with recurrent circuits involving connections with other motor unit pools. This study clarifies an important debated issue in motor unit control by showing that motor unit firings can lie in a multidimensional manifold; however, it may still be impossible for the central nervous system to flexibly control these motor units.

Keywords: motor neuron, synergy, factor analysis, muscle, electromyography

Significant statement. To generate movement, the central nervous system distributes both excitatory and inhibitory inputs to the motor units. The level of flexibility in the neural control of these motor units remains a topic of debate with significant implications for understanding the smallest level of movement control. In this study, by combining experimental data and in silico models, we demonstrated that the activity of a large sample of motor units from a single muscle can be represented by a multidimensional linear manifold; however, these units show very limited flexibility in their recruitment. This is compatible with the presence of a single common input of cortical origin along with recurrent circuits involving connections with other pools, potentially including synergist muscles.

1. Introduction

To generate movement, the central nervous system distributes excitatory and inhibitory inputs to the spinal motor neurons. Observations of correlated or synchronized activity among motor units have led to the assumption that a substantial portion of the net excitatory input is shared across different motor units from the same pool (1–3). The combination of common inputs with the size principle (4) theoretically imposes rigid control on motor units, which is characterized by a consistent size-ordered recruitment pattern. Although this control strategy is computationally efficient at simplifying the neural control of motor units, it has been challenged by a more flexible control, with apparent deviations from the size principle (5–9). Understanding the flexibility in motor unit recruitment requires the identification of the distribution of common inputs (10, 11).

One approach for identifying the structure of common inputs to motor units is to apply linear dimensionality reduction methods to a series of firing times for many units. This approach can capture common patterns in the firing activities of motor units within low-dimensional manifolds shaped by the dynamics of latent factors. Using this approach, the firing patterns of the motor units of certain muscles have been projected onto multidimensional manifolds (12–14). Such a multidimensional manifold of motor unit firings can be interpreted as the presence of multiple common inputs (11). This observation may align with the concept of task-dependent behavior of motor units, and thus it may support flexibility in motor unit control, possibly of cortical origin (8). Although this interpretation is plausible, the neural pathways responsible for increasing the dimensionality of motor unit manifolds remain unclear. Indeed, motor neurons receive numerous excitatory and inhibitory inputs from both cortical and subcortical sources. For example, a multidimensional manifold may result from a single common input of a cortical origin and other common inputs from subcortical sources. This could explain the contradictory results among studies. For example, Bracklein et al. (15) observed that participants could not independently control the motor units of the tibialis anterior muscle, whereas Ricotta et al. (14) showed that the motor unit firings in this muscle lie in a multi-dimensional linear manifold.

In the present study, we hypothesized that common cortical projections to motor neurons are not necessarily the sole inputs that determine the dimensionality of the motor unit manifolds. Other types of inputs, not under direct cortical control, may also shape manifold's dimensionality. For example, the activity of Renshaw cells, which are activated by recurrent collaterals of homonymous and heteronymous motor neurons (16, 17), can contribute in

decorrelating motor unit activity (18). Therefore, this circuit can contribute to increasing the dimensionality of the firing manifold, without increasing the flexibility of the motor unit control. We assume that the flexible control of motor units is primarily determined by the number of common cortical inputs, rather than by the total number of inputs shaping the dimensionality of the manifold. It is possible that, in some muscles, a multidimensional linear manifold underlies a single cortical input, resulting in a rigid control of motor units.

To test this hypothesis, we recorded large samples of motor units to unravel the low-dimensional structures of their inputs. We selected two lower limb muscles, the vastus lateralis (VL) and gastrocnemius medialis (GM), because of their different levels of correlated activity, with the motor units of the VL exhibiting less correlated activity (19) than those of the GM (20). Moreover, crucially for muscle selection, the VL and GM likely have different levels of recurrent inhibition, as animal studies have shown that distal muscles generally exhibit less recurrent inhibition than proximal muscles (21, 22). In this context, we investigated whether the expected difference in manifold dimensionality between the two muscles reflected different levels of flexibility in their motor unit activity, and therefore, different neural constraints on motor unit control. First, we assessed the dimensionality of the manifolds underlying motor unit activity during torque-matched isometric contractions. We then investigated the flexibility in motor unit control under two conditions: sinusoidal contractions with torque feedback and online control with visual feedback on motor unit firing rates. Despite the differences in linear manifold dimensionality between the muscles, both exhibited similar and very limited flexibility in motor unit control. Finally, we developed a simulation model that demonstrated that the multidimensionality of the linear manifold in the VL was compatible with the presence of a single descending drive of cortical origin, with a modular distribution of both homonymous and heteronomous recurrent inhibition. These results support different sources of common inputs projecting to the VL motor units; however, not all are under volitional control. This study clarifies an important debated issue in motor unit control, by showing that motor unit firings can lie in a multidimensional manifold; however, it may still be impossible for the central nervous system to flexibly control these motor units.

2. Results

2.1. Experiment 1: force-matched contractions

Thirteen participants performed either isometric knee extension (n=7) or plantarflexion (n=6) tasks. These tasks consisted of matching either a trapezoidal target at 20% maximal voluntary contraction (MVC, referred to as "reference" contractions), or a sinusoidal target oscillating between 15% and 25% MVC at three different frequencies: 0.25, 1, and 3 Hz (referred to as "sinusoidal" contractions). Electromyographic (EMG) signals were recorded with four grids of 64 surface electrodes (a total of 256 electrodes) placed over the vastus lateralis (VL) during the knee extension tasks or the gastrocnemius medialis (GM) during plantarflexion tasks. During the knee extension tasks, EMG signals were also recorded from the rectus femoris (RF) and vastus medialis (VM), with one grid of 64 surface electrodes over each muscle. A blind source-separation algorithm (23) was applied on to the EMG signals to identify motor units spike trains. Using multiple grids of electrodes per muscle optimized the spatial sampling of motor unit surface action potentials (24), resulting in a large sample of identified motor units (VL: up to 60 motor units/participant and GM: up to 67 motor units/participant).

2.1.1. Low-dimensional analysis

We applied a linear dimensionality reduction method, as classically done to characterize the dynamics of populations of neurons (25–28). In our study, dimensionality reduction was applied to the firing rates of the detected motor units to identify a low-dimensional latent space. Specifically, we conducted a factor analysis of the motor units that continuously fired during the plateau phase of the reference contractions (Fig. 1). This analysis included an average of 38.1 ± 8.1 (range: 26-48) motor units per participant for the VL, and 28.0 ± 19.8 (range: 9-60) motor units per participant for the GM. To determine the dimensionality of the latent space, we identified the number of latent factors beyond which adding another factor did not improve the model's ability to reconstruct the data more than would be expected from fitting random noise (29). Using this approach, we identified three latent factors in the VL muscle for all participants, accounting for 55% ± 7% (range: 43%-65%) of the total variance in motor unit firing rates. When considering the GM muscle, only one latent factor was identified in five out of six participants, accounting for 69% ± 11% (range: 52%-82%) of the total variance. Two latent factors were identified for the remaining participant, accounting for 60% of the total variance. Notably, we also used alternative methods to determine the number of latent variables

(30, 31), which yielded the same results (see the Methods section). These results indicate a distinct dimensionality of the latent spaces of the VL and GM muscles, as suggested by previous work (12, 32).

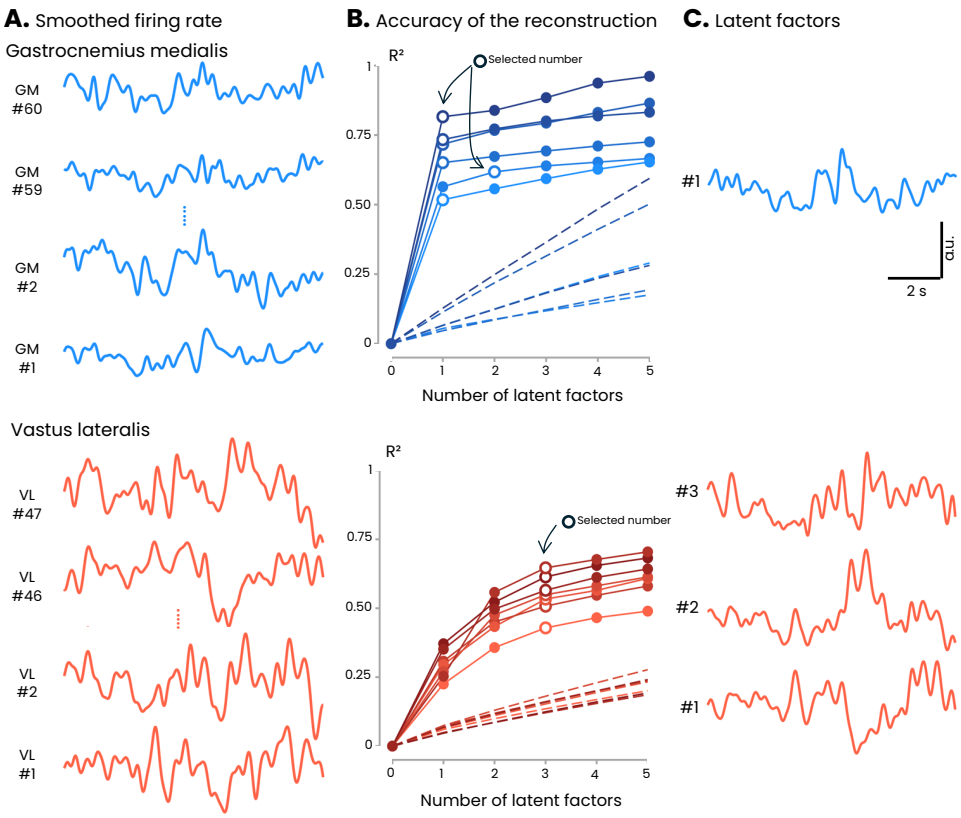

Figure 1 – Dimensionality of motor unit behavior. (A) Individual example of the smoothed firing rate of motor units identified in the GM (Gastrocnemius medialis, upper panel) and the VL (vastus lateralis, lower panel). In these individual participants, 60 motor units were identified in the GM and 47 in the VL. These patterns of smoothed firing rates were used as input to the factor analysis. (B) For each number of latent factors (1 to 10, only 5 of which are shown here), we calculated the reconstruction accuracy as the r-squared between the reconstructed and the original data. Each participant is represented by a different shade of blue/red. The dashed lines represent the variance explained for the surrogate data obtained by shuffling the inter-spike intervals of the recorded motor units (see Methods). The number of identified latent factors (dots filled in white) corresponds to the number of latent factors after which the slope of the r-squared curve from experimental data becomes lower than the slope of the R^2 from the surrogate data. (C) Identified latent factors for an individual participant. a.u. arbitrary unit.

2.1.2. Flexibility in the motor unit control

Based on recent work reporting flexibility in recruitment during sinusoidal tasks (8), we evaluated the motor unit recruitment during isometric contractions with sinusoidal force profiles at various frequencies. Specifically, flexibility was quantified using two metrics:

dispersion and *displacement* (8) (Fig. 2). The rationale for using these metrics is based on the premise that the rigid control of motor units by a single common input would constrain the trajectory of their firing rate along a 1-dimensional (1-D) monotonic manifold. Whereas small deviations from this monotonic 1-D manifold would reflect the presence of synaptic noise, large deviations would imply that the motor units receive different inputs, resulting in a certain level of flexibility. These two metrics are formally defined in the Methods section. Considering the three contraction frequencies, this analysis included a mean of 39.2 ± 7.6 motor units per participant for the VL (mean number of pairs: 5723 ± 1862), and 27.5 ± 16.9 (total number of pairs: 3854 ± 3364) motor units per participant for the GM.

In this paragraph, "motor unit pairs" (GM-GM and VL-VL) refers to the *Muscle* effect, while the "frequency of the sinusoidal contractions" (0.25, 1, and 3 Hz) refers to the *Contraction* effect. Although there was no significant main effect of *Muscle* on either *dispersion* ($p=0.28$) or *displacement* ($p=0.85$), we did observe a significant main effect of *Frequency* ($p<0.001$ for both metrics), as well as a significant interaction between *Muscle* and *Contraction* ($p=0.001$ for both metrics). For the sake of clarity, we present only the differences between muscles that are directly relevant to our main objective. There was no difference between the GM and VL neither for *dispersion* nor for *displacement* in all conditions (all $p>0.09$), except for the 1-Hz sinusoidal contraction, during which the GM motor units displayed higher dispersion ($p<0.001$) and higher displacement ($p<0.001$) than the VL motor units (Fig. 2). Further, we noted no significant correlation between the distance separating the two motor units on the skin surface (as evaluated from their action potentials across the four grids) and the degree of flexibility, as measured using *dispersion* (mean r value across participants/conditions: 0.002±0.071, $p=0.11$) or *displacement* ($r=-0.004\pm0.066$, $p=0.29$).

To determine whether the level of flexibility estimated through *dispersion* and *displacement* was significant or negligible, we calculated both metrics for pairs of motor units in the RF and VL muscles. Given that the RF muscle is biarticular, and can be activated independently of the vastus muscles (33), the *displacement* and *dispersion* values for pairs of RF-VL motor units were considered to provide insights into the expected degree of flexibility of motor units that receive different inputs. From a relatively low number of units identified in the RF (5.4±4.6 motor units per participants), we identified a higher flexibility for pairs involving RF compared to the VL-VL or GM-GM pairs (dispersion: +20% and +6% for RF-VL compared to VL-VL and GM-GM across the three conditions, respectively; displacement: +32% and +19% for RF-

VL compared to VL-VL and GM-GM across the three conditions, respectively). This suggests that the flexibility observed in both the VL and GM motor units was comparatively small, even though the factor analysis identified three latent factors for the VL.

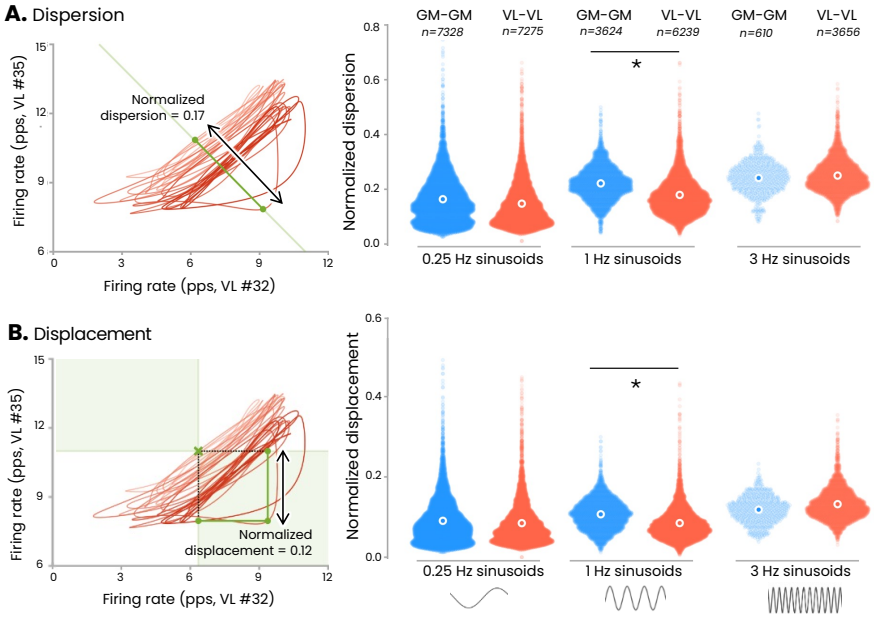

Figure 2 – Motor unit recruitment flexibility during sinusoidal tasks. We evaluated the flexibility in motor unit recruitment during isometric contractions with sinusoidal force profiles at various frequencies (0.25, 1, and 3 Hz). To achieve this, we quantified flexibility using two metrics: *dispersion* and *displacement* (8). The rationale for using these metrics is based on the premise that the rigid control of motor units would constrain the trajectory of their firing rate along a one-dimensional monotonic manifold (see Methods). The right panels display the normalized values of the dispersion and displacement for each tested pair of GM-GM and VL-VL motor units (*n* is indicated on top). White circles represent the mean value. There was no difference between muscles, except for the 1 Hz condition, where GM-GM pairs exhibited a slightly higher flexibility than the VL-VL pairs. GM, gastrocnemius medialis; VL, Vastus lateralis; pps, pulse per second.

2.2. Experiment 2: Volitional control of motor units

We performed a second experiment to determine whether the distinct behaviors of the VL and GM motor units reflected a distinct dimensionality of their *volitional* control. Specifically, we assessed whether the participants were able to volitionally dissociate the activity of two motor units when presented with online visual feedback of their firing rates. Participants performed either isometric plantarflexion (n = 5) or knee extension tasks (n = 5). During these tasks, we recorded the EMG signals from either the GM for the plantarflexion task or the VL for the knee extension task. Two surface grids, each comprising 64 electrodes (a total of 128 electrodes per muscle), were positioned over the proximal and distal regions of each muscle. The feedback

provided to the participants included one motor unit from each of the two grids, which provided them with information about the location of the motor units they were asked to control. Visual feedback involved a cursor navigating in a 2-D space, where the cursor coordinates corresponded to the firing rates of the two motor units. Two target areas along the x- (Target 1) or y-axes (Target 2) were displayed to the participants (Fig. 3). To position the cursor within these target areas, the participants had to modulate the firing rates of the two motor units independently, that is, increase the firing rate of one unit while maintaining or decreasing the firing rate of the other unit. We tested an average of 2.6±0.5 (VL) and 1.8±0.8 (GM) pairs of motor units per participant (total of 13 pairs for VL and 9 pairs for GM). For each pair of motor units, the participants performed two sets of 10-seconds contractions at either 10% (VL) or 20% MVC (GM). Participants were instructed to reach Target 2 during the first set, and target 1 during the second set. The success rate was calculated as the percentage of time for which the participants maintained the cursor within the targets while producing the required torque (with a margin of +/- 5%) over the total duration of the contraction. For the purposes of analysis, the firing rate of the motor unit with the highest recruitment threshold was depicted on the *y*-coordinate (Target 2). Reaching Target 2 suggests that the participants successfully isolated the activation of the highest threshold unit, which supports a flexible control. The success rate associated with Target 1 was 30.4±32.4% for VL and 27.1±23.9% for GM. Interestingly, none of the participants were able to reach Target 2, regardless of the muscle (success rate = 0%).

We further analyzed the behavior of the motor units that were not displayed as feedback to the participants (15.6±7.1 motor units per participant for the VL and 16.6±6.2 motor units per participant for the GM). In very rare cases, we found that Target 2 was reached by these motor units, but with no difference between the two muscles (3.0±12.8% of total time for VL and 3.4±14.0% of total time for GM (p=0.41, t-test). Together, these results support a lack of flexibility in the volitional control of the motor units of the GM or VL muscles, despite the distinct dimensionality of their manifolds. This conclusion contrasts with the expectation that a greater dimensionality would correspond to a greater number of common inputs of cortico-spinal origin (8). Therefore, we analyzed other mechanisms that might explain the experimental observation of rigid control with the presence of multiple latent factors in the VL.

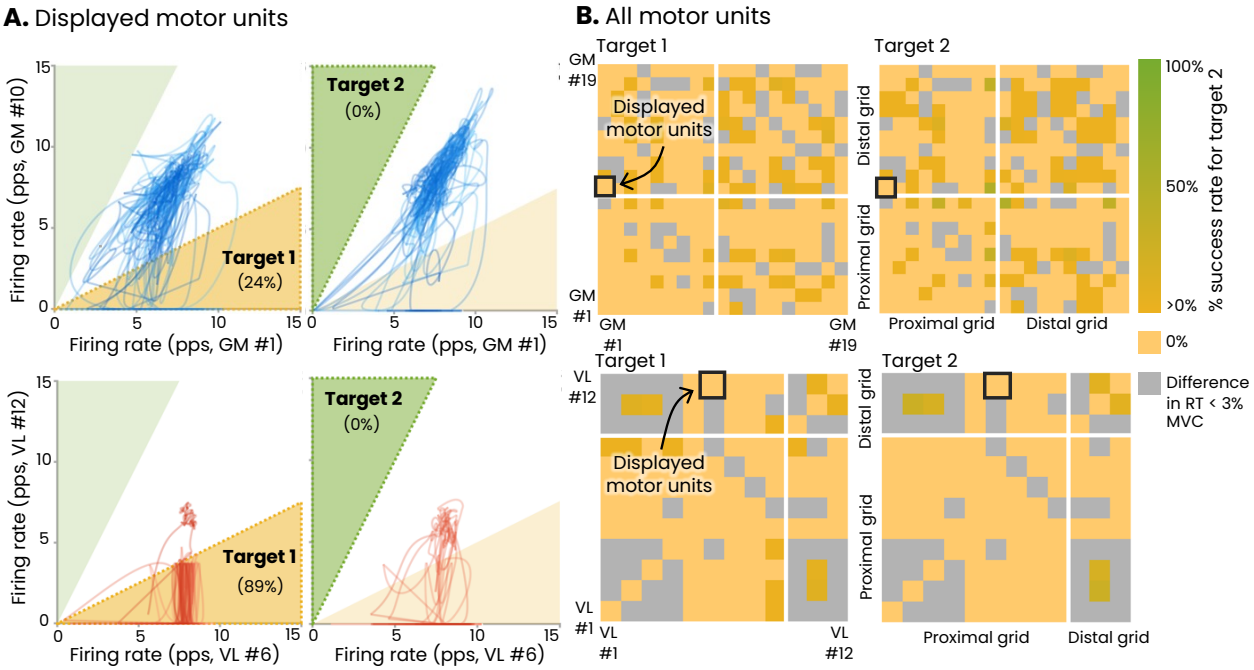

Figure 3 – The online control task with visual feedback. This figure illustrates the results obtained for one representative participant for both the gastrocnemius medialis (GM, top panels) and the vastus lateralis (VL, bottom panels). (A) The visual feedback involved a cursor navigating in a 2-D space, where the cursor coordinates corresponded to the firing rates of the two motor units. Two target areas, along the x- (Target 1) or y-axes (Target 2), were displayed to the participants. The dark shaded area represents the target the participant was instructed to reach, with the success rate (% of time spent in this target) indicated in parentheses. Note that the firing rate of the motor unit with the highest recruitment threshold is depicted on the *y*-axis (Target 2). Flexible control, which corresponds to deviations from the size principle, is demonstrated by the ability to reach Target 2, which was not achieved in this participant. (B) For all the other pairs of motor units identified during this task, but not depicted as feedback, we calculated the success rate as the percentage of time during which the higher threshold motor units had a firing rate twice as high as the lower threshold motor units. This condition is equivalent to reaching Target 2. This analysis was only performed for pairs of motor units with a difference in recruitment threshold > 3% of maximal voluntary contraction (MVC; see Methods). The pair indicated as 'displayed motor units' are the pairs provided as feedback on Panel A. The vast majority of motor units showed a success rate of 0%. RT, recruitment threshold; pps, pulse per second.

2.3. In-silico models with spiking neural networks

We developed in-silico models to gain further insights into the control mechanisms that might explain the differences observed between the GM and VL. Specifically, we tested scenarios of input distribution compatible with the multidimensionality of the linear manifold underlying the behavior of VL motor units. We identified recurrent inhibition as a potential mechanism that could introduce non-linearity into the dynamics of motor unit population (16, 18, 34, 35). It has also been proposed that recurrent inhibition is topographically organized and affects both homonymous and heteronymous motor neuron pools (36, 37).

297 Overall, we simulated three pools of 50 leaky integrate-and-fire motor neurons, representing
298 the motor neurons from three distinct pools, which could correspond to the VL, VM, and Vastus
299 Intermedius muscles. Each pool was associated with ten Renshaw cells that delivered recurrent
300 inhibition to the homonymous and heteronymous motor neurons (Fig. 4). Four scenarios were
301 tested, as follows: 1) a single common excitatory input to all motor neurons innervating a given
302 pool, without any recurrent inhibition (hereinafter referred to as the "control scenario"); 2)
303 three common excitatory inputs distributed heterogeneously to the motor neuron pools, such
304 that each pool received all three inputs, without any recurrent inhibition (referred to as the
305 "multiple common excitatory inputs scenario"); 3) a single common excitatory input to all
306 motor neurons innervating a given pool, with homonymous recurrent inhibition randomly
307 distributed within each pool (referred to as the 'homonymous recurrent inhibition' scenario);
308 and 4) a single common excitatory input to all motor neurons innervating a given pool, with
309 specific modules of homonymous and heteronymous recurrent inhibition (referred to as the
310 'homonymous and heteronymous recurrent inhibition' scenario). In these scenarios, the inputs
311 to each pool were different, but well correlated to account for the relatively high level of
312 common inputs reported between the vastii muscles (38). These simulations generated 20 s of
313 motor neuron firing activity, and each scenario was simulated seven times using different
314 excitatory inputs derived from the experimental data of each participant (see Methods).

315 Factor analysis was applied to the activity of the in-silico motor neurons to estimate the
316 dimensionality of their linear manifolds in the same manner as the experimental data. The
317 control scenario resulted in the identification of only one latent factor, confirming that a pool
318 of motor neurons acts approximately linearly to transmit these common inputs (2, 39). In
319 contrast, the three other scenarios consistently resulted in the identification of multiple latent
320 factors: three latent factors in all seven simulations for the 'multiple common inputs' scenario,
321 an average of 1.7±0.5 latent factors (one and two latent factors in four and three cases,
322 respectively) for the 'homonymous recurrent inhibition' scenario, and an average of 3.1±0.4
323 latent factors (three and four latent factors in six and one case, respectively) for the
324 'homonymous and heteronymous recurrent inhibition' scenario (Fig. 4). Taken together, these
325 results indicate that the multidimensionality of the linear manifold observed in the experimental
326 VL data is compatible with the presence of one excitatory input commonly projected onto the
327 pool of motor units, and the presence of recurrent inhibition. However, for this
328 multidimensionality to emerge, recurrent inhibition must involve connections between

heteronymous muscles and must project onto a substantial number of motor neurons to provide additional common inputs. Indeed, the 'homonymous recurrent inhibition' scenario led to an overall decrease in r-squared (Fig. 4), without adding a significant amount of latent factors.

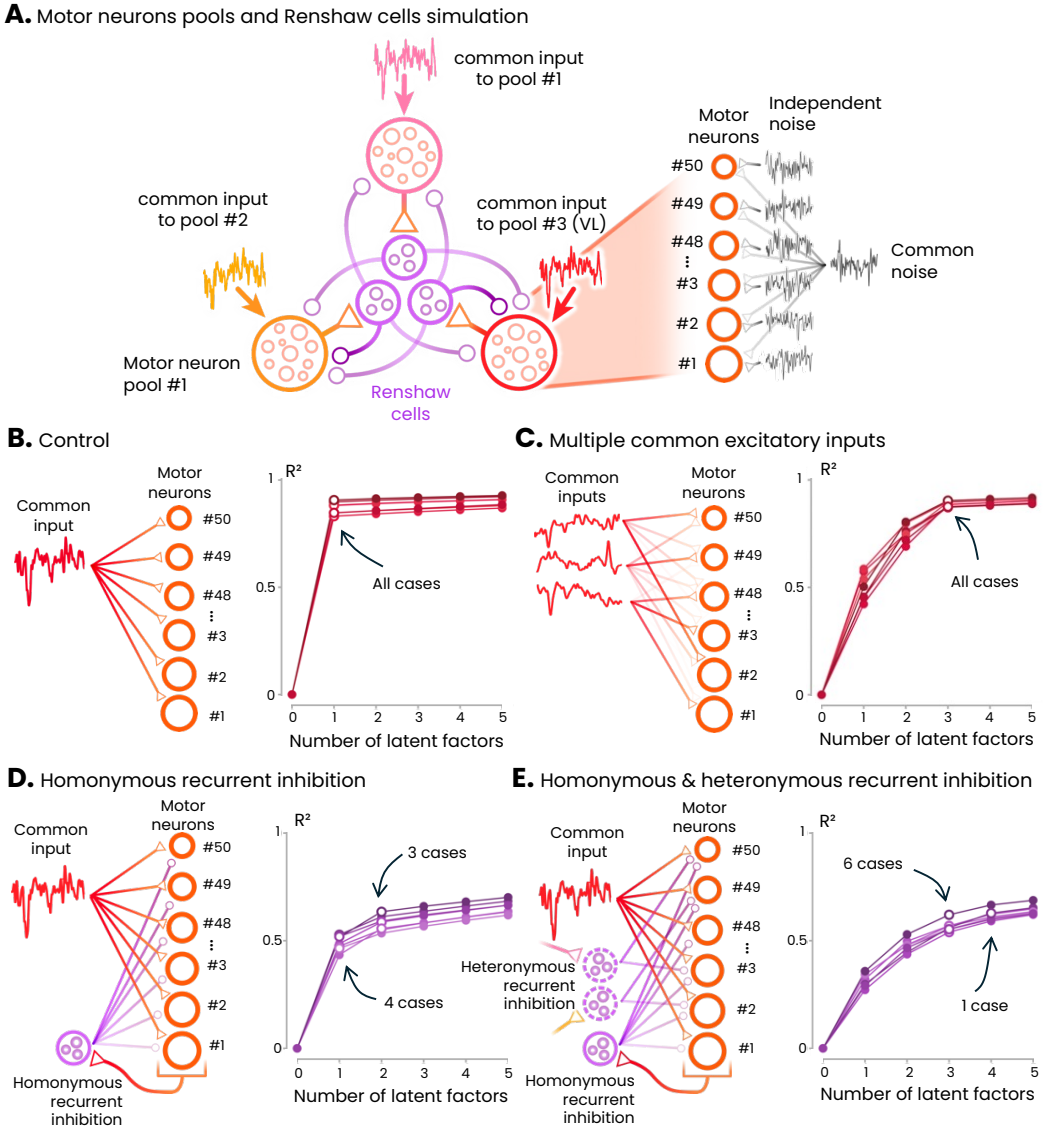

Figure 4 – Simulation scenarios. (A) Schematic representation of the spiking neural network structure. We simulated 3 pools of 50 motor neurons and 3 groups of 10 Renshaw cells. All motor neurons within each pool received both a common input (0-5 Hz bandwidth) and common noise (0-10 Hz bandwidth). In addition, each motor neuron received independent noise (0-50 Hz bandwidth). The common inputs distributed to each of the three pools were not identical, but correlated with each other (mean r across simulations: 0.70) to reproduce the high level of common drive observed between the vastii (38). Each group of Renshaw cells received excitatory input from homonymous motor neurons and sent inhibitory input back to all pools, but with a higher connectivity ratio for the homonymous pool, as indicated by the increased edge opacity. We simulated four scenarios, each performed 7 times, using different excitatory inputs derived from each participant's experimental data. A factor analysis was applied on one pool; **(B)** all motor neurons received the same common input, without recurrent inhibition, resulting in the identification of one latent factor; **(C)** each motor neuron of the pool received three excitatory

common inputs orthogonal to each other, without recurrent inhibition, resulting in the identification of 3 latent factors; (**D**) All motor neurons received the same common input, while only the homonymous Renshaw cells had an effect on these motor neurons. The decreasing opacity of the edges indicates that larger motor neurons received less inhibitory input than smaller motor neurons (see Methods), leading to the identification of either 1 or 2 latent factors; (**E**) all motor neurons received the same common input and received both homonymous and heteronymous recurrent inhibition. The Renshaw cells-to-motor neurons connections of the heteronymous modules were non-overlapping, and their proportion was set to one-third of the connectivity of the homonymous module of Renshaw cells (see Methods). This scenario resulted in a higher dimensionality of the linear manifold, with either 3 or 4 latent factors

3. Discussion

We investigated the low-dimensional structure of the motor unit activity in two lower limb muscles. By applying a linear dimensionality reduction approach applied to a large sample of motor units, we found that the activity of the GM motor units was effectively captured by a single latent factor defining a unidimensional manifold, whereas the VL motor units were better represented by three latent factors defining a multidimensional manifold. Despite this apparent difference in the dimensionality of the manifolds, the recruitment of motor units in the two muscles exhibited similarly limited levels of flexibility. Using a spiking network model, we propose that VL motor unit behaviors can be explained by the combination of a single common input of cortical origin with recurrent circuits involving connections with other pools (possibly synergist muscles). Taken together, these results suggest that the dimensionality of motor unit linear manifolds is determined by inputs from both cortical and subcortical sources.

There is evidence from anatomically compartmentalized muscles that synchronization between motor units is stronger within muscle compartments than between compartments (40–42). Recent studies have further extended this observation to non-compartmentalized muscles, demonstrating that the behavior of motor units is more accurately represented by multidimensional linear manifolds (11–14). These results align well with our finding that three latent factors are required to explain the variance in VL motor unit activity. Although this could be explained theoretically by the presence of multiple independent corticospinal drives projecting to a single pool (8, 11), our results for the VL muscle do not support this hypothesis. Indeed, we showed that none of the participants could volitionally dissociate the activity of pairs of VL motor units. Furthermore, despite previous studies indicating that tasks with rapid changes in force can trigger flexibility in motor unit recruitment (8, 43), we did not observe any higher flexibility in the VL than in the GM during the fast oscillation tasks. Together, these findings indicate that multidimensionality in motor unit firing manifolds does not necessarily imply the presence of multiple cortical inputs, and is therefore not a sufficient condition for flexible control. Interestingly, although several studies have previously reported multidimensional manifolds of the firings of motor units within (14) and across muscles (44), none have demonstrated clear flexible control in humans under constrained conditions (45).

If the difference in dimensionality in the manifolds for the VL and GM is not due to a different number of cortical inputs, as suggested by the lack of flexibility in control, then a question arises as to how to explain this difference in dimensionality. Among the various neural pathways involved in the control of motor units, recurrent inhibition by Renshaw cells likely plays a crucial role in the behavior observed in VL motor units. The role of Renshaw cells in decorrelating the activity of motor units within a pool has been previously discussed in other contexts (16, 18, 21, 35). Moreover, several prior studies have discussed the role of recurrent inhibition, involving between-muscle connections (46), in shaping the commonality in firing rates of motor units by distributing the same inhibition to large groups of motor neurons (18, 47). While some of these results may appear contradictory, they could all be interpreted based on the different implications that different sources of common input to motor neurons have on the neural constraints of motor unit control. For example, while recurrent inhibition may contribute to decorrelating motor unit firings within the same pool, it may also contribute to correlating the activity between distinct pools linked by strong mutual recurrent inhibition (47).

We used a spiking neural network model to test the hypothesis that the dynamics of the VL motor units are compatible with greater effect of recurrent inhibition, involving both homonymous and heteronymous pathways, than the GM. We found that even with a single cortical drive projecting to the full pool of motor units, the dimensionality of the manifold underlying motor unit behavior increased with the addition of recurrent inhibition to the model. Interestingly, a better fit to our experimental data was achieved when the model not only incorporated homonymous recurrent inhibition, but also heteronymous recurrent inhibition. This was in the form of distinct inhibitory inputs driven by synergist muscles, which in our case were putatively the vastus medialis and vastus intermedius muscles. This finding is consistent with observations in previous studies showing that Renshaw cells can be activated by recurrent collaterals of synergist motor neurons (17, 21, 48). Such organization of recurrent inhibition within the quadriceps muscle group may explain both the relatively high correlation of activity between motor units from the VL and VM (19, 38), and the relatively low correlation between motor units within each muscle (19) compared to other muscles (e.g., GM: (20)). Higher recurrent inhibition in the VL (and, by extension, within the quadriceps muscle group) than in the GM muscle aligns with studies showing a proximo-distal gradient of recurrent inhibition and motor unit synchronization, with higher recurrent inhibition in proximal muscles

than in distal muscles (21, 48–51) and higher synchronization in the distal muscles than in proximal muscles (52).

Uncorrelated modulation of the motor unit firing rate is filtered out in the net output to the muscle. As such, fine-tuning the muscle force requires a substantial level of correlation across motor units (2, 39). Although this may initially suggest that the VL motor units control scheme is less effective, it is important to consider that the motor units of the VL still receive a substantial portion of common cortical inputs (53), and that the VL and VM motor units share a large proportion of common input, resulting in correlated activity between the two muscles (19, 38). This shared input could mean that the Vastii muscles are more effective at controlling the force as a group. Although we cannot exclude the possibility that the decorrelation of the VL motor unit activity through recurrent inhibition is an epiphenomenon arising from the complex circuitry of motor pathways serving no functional role, it seems improbable that biological systems would evolve sub-optimal muscle control schemes. Therefore, we argue that the distinct control schemes of the GM and VL are designed to comply with specific functional roles. While the VL works in combination with the VM to primarily extend the knee, these two muscles also stabilize the patella with opposite mechanical actions. As such, appropriate coordination between the VL and VM is required to regulate internal joint stresses (54). In this way, recurrent inhibition between these pools can help to fine-tune the force on the patella, while a single drive controls the knee extension torque. In contrast, the gastrocnemii share little common inputs (20), thus allowing these muscles to be controlled independently to comply with secondary task goals, such as stabilizing the ankle joint in the frontal plane. Together, these results support the functional role of recurrent inhibition and the idea that it is large for motor nuclei with consistent activity patterns, whereas it is absent or moderate for motor nuclei that are activated independently (55).

Although our simulation results support the possibility that recurrent inhibition can explain the distinct dimensionality of the linear manifolds underlying the behavior of the VL and GM motor units, we cannot exclude the possibility of contributions from other neural pathways with recurrent connections. For example, the distribution of Ia afferents to motor neurons within and between synergist muscles (46) suggests that Ia excitation could introduce additional common excitatory drives. If the distribution of the Ia excitation inputs to the motor

units is similar to that simulated in our in-silico model, these additional drives may increase the dimensionality of the linear manifold. However, experimental evidence for this is lacking (47, 56). Nevertheless, this potential limitation does not affect our main conclusion that the multidimensionality of motor unit linear manifolds does not necessarily imply independent common inputs of cortical origin. Specifically, the present study addresses a key debated issue in motor control by demonstrating that, although motor unit firing can reside in a multidimensional manifold, it may be impossible for the central nervous system to flexibly control these motor units.

4. Methods

4.1. Participants and ethical approval

The first experiment involved a series of isometric force-matched knee extension and plantarflexion tasks. Nine physically active males (age: 26.7±7.6 years, height: 179.7±7.9 cm, body mass: 76.6±11.6 kg) performed the knee extension tasks while seven active males (age: 29.2±7.2 years, height: 176.8±2.8 cm, body mass: 77.8±10.1 kg) performed the plantarflexion tasks. Two participants performed both the knee extension and plantarflexion tasks in two separate sessions. Owing to the low number of identified motor units (typically fewer than 10), two participants were excluded from the analysis of the knee extension task, and one participant was excluded from the plantarflexion task.

The second experiment involved isometric knee extension or plantarflexion tasks, during which the participants controlled the activity of pairs of motor units using online visual feedback on their firing rate. Six physically active males performed the knee extension tasks (age: 29.2±7.9 years, height: 175.2 ±3.1 cm, body mass: 73.8±8.6 kg) and the plantarflexion tasks (age: 29.4±7.7 years, height: 176.2±3.9 cm, body mass: 74.8±8.4 kg). Five of these participants completed both tasks across two separate sessions.

Participants had no history of lower leg pain with limited function that required time off work or physical activity, or a consultation with a health practitioner in the previous 6 months. The procedures were approved by the ethics committee (CPP Ouest III; 23.00453.000166), and were performed according to the Declaration of Helsinki, except for registration in a database. The participants were fully informed of any risks or discomfort associated with the procedures before providing written informed consent.

4.2. Experimental design

For the knee extension tasks, the participants sat on a dynamometer (S2P Ltd, Ljubljana, Slovenia, EN 60204-1) with their hips and right leg each flexed at 80° (0° being the neutral position). For the plantarflexion tasks, the participants sat on a dynamometer (Biodex System 3 Pro, Biodex Medical, USA) with their hips flexed at 80° and their right legs fully extended. The foot was placed perpendicular to the shank. During both tasks, inextensible straps were tightened to immobilize the torso, pelvis, and thighs on the test side. These isometric tasks were used in the two experiments. In the first experiment, the participants matched the visual torque

feedback. In the second experiment, they aimed to modulate the activity of two motor units using online visual feedback displaying their firing rates. In both experiments, sessions began with a standardized warm up, followed by three maximal voluntary contractions (MVC) for 3 s, with 60 s of rest in between. Peak MVC torque was considered as the maximal value obtained from a moving average window of 250 ms.

4.2.1. Experiment 1 (torque-matched contractions)

Participants performed four trapezoid isometric contractions, each consisting of a 10-s linear ramp up, a 30-s plateau at 20% MVC, and a 10-s linear ramp down, with 30-s of rest in between. Participants then performed sinusoidal contractions, producing torque oscillations at frequencies of either 0.25 Hz, 1 Hz, and 3 Hz. Each sinusoidal contraction consisted of a 5-s linear ramp up to 20% MVC, followed by a 10-s plateau at 20% MVC, and 20 s of sinusoidal oscillations between 15% and 25% MVC. Each sinusoidal contraction was performed three times, with at least 60 s of rest in between. The order of the frequency conditions was intentionally not randomized to allow the participants to progressively familiarize themselves with faster oscillations. For the 3 Hz sinusoidal condition, auditory feedback was provided in addition to visual feedback using a metronome.

4.2.2. Experiment 2 (Volitional control of motor units)

Participants performed a trapezoid isometric contraction consisting of a 5-s linear ramp up, a 20-s plateau at either 10% (knee extension) or 20% MVC (plantarflexion), and a 5-s linear ramp down (referred to as 'baseline' contraction). This baseline contraction was used to identify motor unit separation vectors (filters) offline, which were then reapplied in real-time to display the motor unit firing rate as a visual feedback (57). After a 15-30 min rest period during which automatic offline EMG decomposition and manual editing of the motor units were performed, the participants performed four 20-s submaximal isometric contractions, with 1-min of rest in between. Only the torque feedback was provided to the participants during these contractions (referred to as "reference" contractions).

The rest of the experimental session consisted of a series of 10-s isometric contractions during which the participants were instructed to dissociate the activity of two motor units while maintaining constant knee extension (10% MVC) or plantarflexion (20% MVC) torque constant. Specifically, the activity of the two motor units was depicted in 2D space, where the *x*- and *y*- axes represented the firing rates of motor units #1 and #2, respectively. The scale of

522 each axis ranged from 0 to twice the average firing rate of the corresponding motor units
523 measured during baseline contraction. This scaling ensured that the cursor was not biased
524 towards any of the axes. Two target triangles were added to the 2D space, each with one corner
525 on the coordinate origin and two sides as one axis (*x* or *y*), and a line forming an angle of 30°
526 along this axis. In addition, real-time feedback on torque output was provided to the
527 participants *via* a vertical gauge, which they were required to maintain within two lines
528 representing ±5% of the target torque.

529 For a given pair of motor units, the participants performed two sets of ten 10-s contractions,
530 with 10 s of rest between each contraction. The participants aimed to reach Targets 2 and 1
531 during the first and second sets, respectively. To move the cursor towards these targets, the
532 participants were required to differentially alter the firing rates of the two motor units (i.e., an
533 increase in one unit with no change or a decrease in the other unit). This procedure was repeated
534 with two to four different pairs of motor units, depending on the participant. Each pair
535 comprised a motor unit from each of the two EMG grids (proximal and distal), providing
536 participants with information regarding the location of the motor units they were asked to
537 control independently.
538

539 **4.3. Decoding of motor unit firing activity**

540 *4.3.1. High-density surface electromyographic recordings*

541 EMG signals were recorded from either the GM (plantarflexion) or the VL, RF, and VM (knee
542 extension). For the first experiment, four adhesive grids of 64 electrodes (total of 256
543 electrodes) were placed over the VL (inter-electrode distance: 8 mm; GR08MM1305, OT
544 Bioelettronica, Italy) or GM (inter-electrode distance: 4 mm; GR04MM1305, OT
545 Bioelettronica, Italy). One grid each of 64 electrodes was placed over the RF and VM muscles
546 (inter-electrode distance: 8 mm; GR08MM1305, OT Bioelettronica, Italy). For the second
547 experiment, two adhesive grids of 64 electrodes (a total of 128 electrodes) were placed over
548 the VL (inter-electrode distance: 8 mm; GR08MM1305, OT Bioelettronica, Italy) or GM (inter-
549 electrode distance: 4 mm; GR04MM1305, OT Bioelettronica, Italy). This setup was selected
550 to maximize the number of decomposed motor units (Caillet et al., 2023).

551 Prior to electrode application, the skin was shaved and cleaned with an abrasive paste (Nuprep,
552 Weaver and Company, USA). Adhesive grids were held on the skin using bi-adhesive foam
553 layers (SpesMedica, Battipaglia, Italy). The skin-electrode contact was made by filling the

554 cavities of the adhesive layers with conductive paste (SpesMedica, Battipaglia, Italy). A
555 reference electrode (5×5 cm; Kendall Medi-Trace; Covidien, Ireland) was placed over the right
556 patella (knee extension tasks) or right tibia (ankle plantarflexion tasks), and a strap electrode
557 dampened with water (ground electrode) was placed around the left ankle. The EMG signals
558 were recorded in a monopolar montage, bandpass filtered (10–500 Hz), and digitized at a
559 sampling rate of 2048 Hz using a multichannel acquisition system (EMG-Quattrocento; 400-
560 channel EMG amplifier; OT Biolelettronica, Italy).

561 *4.3.2. Offline EMG decomposition and motor unit tracking*

562 The EMG signals were decomposed using convolutive blind source separation (23, 58),
563 implemented in the MUedit software (59). Prior to automatic decomposition, the channels were
564 visually inspected and those with low signal-to-noise ratio or artifacts were discarded. The
565 remaining EMG signals were extended and whitened. A fast independent component analysis
566 was performed to retrieve the motor unit spike trains mixed within the EMG signals.
567 Specifically, a separation vector was optimized for each motor unit using a fixed-point
568 algorithm to obtain a sparse motor unit pulse train. Firing times were identified from these
569 pulse trains using a peak detection function and a k-mean classification that separated the high
570 peaks (the firing times) from the low peaks (noise). The distance between the high and low
571 peaks was quantified using the silhouette value, and only the pulse trains with a high distance
572 between the high and low peaks (threshold: 0.9) were retained for the subsequent analyses. The
573 resulting spike trains were then edited manually. Manual editing is an iterative process that
574 involves removing detected peaks that result in erroneous firing rates (outliers), and adding
575 missed firing times that are clearly distinguishable from the noise. The motor unit pulse trains
576 are ultimately recalculated with updated separation vectors and accepted by the operator once
577 all the putative firing times are selected. This procedure was performed according to the
578 guidelines described by Del Vecchio et al. (60), and was demonstrated to be highly reliable
579 across operators (61).

580 The decomposition was performed independently on each electrode grid. Given that the same
581 motor units could be detected across multiple grids covering the same muscle, duplicate units
582 were identified through analysis of their pulse trains. The pulse trains of pairs of motor units
583 were first aligned using a cross-correlation function to account for a potential delay owing to
584 the propagation time of the action potentials along the fibers. Firing times that occurred within
585 0.5 ms interval were considered as common between motor units; and motor units that shared

more than 30% of their firing times were considered as duplicates (62). When duplicated motor units were identified, only the motor unit with the lowest coefficient of variation of its inter-spike intervals was retained.

For the first experiment, the decomposition procedure described above was performed on each task separately, that is, each trapezoidal reference contraction and each sinusoidal contraction. The motor units were tracked across the four trapezoidal reference contractions. To this end, the separation vectors of the motor unit identified in one contraction were applied to the extended and whitened EMG signals of the other contractions (63). The resulting spike trains were then compared with those obtained after manual editing. A motor unit was tracked if at least 30% of its spikes were shared. This process was applied to each potential pair of contractions. This automatic process was complemented with visual inspection of the 2D spatial distribution of motor unit action potentials across the 256 electrodes to confirm the accuracy of the motor unit tracking. Notably, motor units were not tracked between the reference and sinusoidal contractions due to a decrease in motor unit yield. However, we verified that outcomes remained consistent even with the smaller sample of tracked units (results not reported here).

4.3.3. Real-time EMG decomposition

To provide online feedback on the motor unit activity in the second experiment, the EMG signals were decomposed in real-time using an open-source software developed and validated by our team (57). First, EMG signals were recorded during a submaximal trapezoid contraction and decomposed offline to identify the motor unit separation vectors and the centroids of the classes ‘spikes’ and ‘noise’ were calculated with a peak detection function and k-mean classification. As the accuracy of the online decomposition can be improved by manually editing the offline decomposition results (44), manual editing was performed prior to the real-time portion of the experiment.

For real-time EMG decomposition, motor unit separation vectors were applied to the incoming segments of 125 ms of EMG signals. Peaks closer to the centroid of the ‘spikes’ class than that the ‘noise’ class were considered as firing times. Besides the 125 ms incompressible delay, the computational time for visual feedback was typically less than 15 ms (44). We calculated the firing rate of individual motor units as the sum of spikes over eight consecutive windows of 125 ms. This approach introduced a 500 ms delay in estimating the firing rate, but allowed for smoother and more controllable visual feedback than using instantaneous firing rates (44).

4.4. Data analysis

4.4.1. Factor analysis

We conducted a factor analysis on the smoothed firing rates of the motor units identified from the GM or VL muscle during the reference contractions (experiment 1) using the "factoran()" function in Matlab (R2023b, Mathworks, USA). First, the binary spike trains were convolved with a 400-ms kernel Hanning window without a phase shift (12). This corresponds to a 2.5 Hz low-pass filter, which retains the information relevant to force production (39, 53). Subsequently, the four 20-s force plateaus were concatenated, and only motor units continuously firing, without any pause between two firings longer than 400 ms, were included in the analysis. Finally, the smoothed firing rates were detrended (47).

Factor analysis allows for factor rotation, which maximizes the overall correlation between the original variables and latent factors, without requiring the latent factors to be orthogonal. We used *promax* rotation, which aims to simplify the structure of the loading matrix by maximizing the weight of one factor, while minimizing the weights of other factors for each variable. To determine the appropriate number of latent factors, we adopted the method proposed by Cheung et al. (29). This approach involves selecting the minimal number of latent factors beyond which additional factors do not significantly improve the model's capability to reconstruct the data over what would be expected from fitting random noise. First, we iterated the factor analysis by varying the number of latent factors between one and ten. For each number of latent factors, the reconstruction accuracy was calculated as the r-squared value between the reconstructed and the original data. We also generated a surrogate dataset through a random permutation of the motor unit spike trains. The surrogate dataset had the same number of spikes and the same mean firing rate as the original dataset. We performed factor analysis on this surrogate dataset, and the r-squared value was calculated for each latent factor from one to ten. We determined the slope of the r-squared curve for the surrogate data by fitting a straight line using least squares regression. The critical number of factors was determined as the maximum count at which the slope of the r-squared curve of the original dataset exceeded that of the surrogate data. Beyond this point, we considered that an additional factor captures noise. Notably, we further explored alternative methods for selecting the number of latent factors. One method involved the selection of the number of factors beyond which the increase in r-squared was lower than 5% (31). Another method involved the selection of the number of

factors at which the r-squared curve plateaus, as indicated by a mean square error of the linear fit of less than 10^{-3} (30).

4.4.2. Dispersion and displacement

We calculated two metrics proposed by Marshall et al. (8) to determine whether the firing rates of motor unit populations deviated from the expected behavior of motor units exclusively receiving a 1-D common input: motor unit displacement and dispersion (Fig. 2). The firing rates of a population of motor units receiving a 1-D common input should constantly vary along a 1-D monotonic manifold in the same direction as that of the common input. If the firing rate of one motor unit increases, all other firing rates should either increase, remain at zero because of a later recruitment threshold, or plateau at the same value because of rate saturation. The motor unit displacement quantifies the difference in firing rates between two motor units when the firing rates of the two units vary in opposite directions. For this, we first computed the maximum non-negative changes in the firing rates between two timestamps, t and t', for a population of *n* motor units.

$$\Delta r(t,t') = max(r1,t - r1,t\,', r2,t - r2,t\,', \ldots, rn,t - rn,t\,')$$

If all the motor unit firing rates vary in the same direction, then either $\Delta r(t,t')$ or $\Delta r(t',t)$ should be equal to 0. The displacement d(t) was considered as the minimum value between $\Delta r(t,t')$ and $\Delta r(t',t)$. It is worth noting that we quantified the displacement values while iteratively adding a time lag τ and τ' of up to 25 ms to t and t', respectively, to account for differences in conduction velocities between motor neurons. Therefore, we maintained the minimal displacement value between $\Delta r(t + \tau, t\,' + \tau')$ and $\Delta r(t' + \tau', t + \tau)$. Finally, we considered the displacement d for a population of motor units as the maximum value out of all the time stamps t.

Dispersion quantifies the maximal deviation of variations in firing rates from a 1D manifold at the population level. Thus, the summed firing rates of a population of motor units receiving a 1-D common input, equivalent to its L1-norm $\|r\|$, should always be associated with the same population state, that is, the distribution of firing rates within the population. Any change in L1-norm within a population of motor units for a given norm value l would mean that at least two motor units have different firing rates for the same summed firing rate. The dispersion quantifies the maximal difference between L1-norms for a given norm value λ.

$disp(\lambda) = \max([\![rt1 - rt2]\!])$

We further quantified the dispersion values while iteratively adding time lag vectors τ and τ' of up to 25 ms to the population of the motor units.

Note that we calculated the displacement and dispersion metrics for all possible pairs of motor units. To facilitate the comparison of motor unit flexibility between muscles and motor tasks with different mean firing rates, we normalized the displacement and dispersion values. Normalization was achieved by dividing the values by the sum of the maximum firing rates of the motor units in each pair.

4.4.3. Distance between motor units

To approximate the distance between motor units within the muscle, motor unit action potential waveforms were calculated by spike-trigger-averaging the differential EMG signals over 50 ms windows for each grid of electrodes. The peak-to-peak amplitude of each waveform was calculated, resulting in a 12x5 array of amplitude values for each grid and motor unit. To mitigate the risk of encountering aberrant values due to the presence of artifacts in the EMG signal, we applied a 3x3 box blur kernel to each of the 12x5 arrays. The electrode with the highest amplitude value across the four grids was considered as the approximate location of the motor unit. These positions were then used to calculate the pair-wise distances between the motor units, assuming an 8 mm inter-electrode distance and a 24 mm inter-grid distance.

4.4.4. Recruitment threshold

Recruitment time was defined as the time of the first firing of a series of three firings occurring within a second. For each motor unit, the recruitment threshold was calculated as the average torque (expressed as a percentage of MVC) recorded at the recruitment times across all contractions.

4.5. Spiking neural network model

4.5.1. Neuron properties

We used the Brian2 package implemented in Python (64) to simulate the behavior of motor unit populations receiving homonymous and heteronymous recurrent inhibition. Specifically, we modelled three pools of 50 motoneurons, which were considered to represent the VL, VM, and vastus intermedius muscles. In each pool, ten Renshaw cells received collaterals from the motor neurons and in turn generated recurrent inhibition (Fig. 4). Each neuron had a resting

membrane potential and reset voltage of 0 (arbitrary unit) and a firing threshold of 1. Additionally, each motoneuron within a given pool was assigned a specific size D (soma diameter, in μm), which determined its time constant (τ, in ms) and input resistance (R, in ohms). The input resistance was normalized such that the smallest motor neuron within each pool had an input resistance of R=1 (arbitrary unit). The relationships between motor neuron size and these properties were calculated according to the following equations from Caillet et al. (65):

$\tau = 2.6 \times 10^{-4} \times D^{-1.5}$ (equation 1)

$R = 9.6 \times 10^{-5} \times D^{-2.4}$ (equation 2)

The motoneuron sizes ranged between 50 μm and 100 μm, corresponding to the theoretical minimal and maximal soma diameters of human motoneurons (66). Notably, because we aimed to simulate the motor neurons active during submaximal contractions at 20% MVC, we compressed the size range so that the 50 simulated motor neurons in each pool were distributed between 50 and 60 μm. The time constant of the Renshaw cells was set to 8 ms (18, 35) with a normalized input resistance of 1. The refractory period was set to 5 ms for both the motor neurons (67) and Renshaw cells.

4.5.2. Connectivity of the simulated network

In the 'homonymous and heteronymous recurrent inhibition' scenario, Renshaw cells received excitatory inputs from all the motor neurons of the homonymous pool, with the excitatory post synaptic potential induced by motor neurons set to 0.1 (arbitrary unit). Each motor neuron from a given pool had a 60% chance of receiving inhibitory input from the Renshaw cells of their homonymous pool. Additionally, one-third of the motor neurons had a 60% chance of receiving inhibitory input from the Renshaw cells of the first heteronymous pool, and another third had a 60% chance of receiving inhibitory input from the Renshaw cells of the second heteronymous pool. These proportions and probabilities ensured that each Renshaw cell had, on average, the same proportion of pre-synaptic to post-synaptic connections (one-third). This configuration resulted in three distinct sources of inhibition distributed among motor neurons in each pool (Fig. 4). This distribution scheme aligns with reports suggesting that recurrent inhibition is organized topographically and affects both the homonymous and synergist motor neuron pools (36, 37). In the 'homonymous recurrent inhibition' scenario, all Renshaw cells had a 33.3%

chance of receiving excitatory input from any motor neuron, and 33.3% chance of sending inhibitory input to any motor neuron, irrespective of the pool.

The inhibitory post-synaptic potential induced by the Renshaw cells was set to -0.05 (arbitrary unit) for the scenarios with recurrent inhibition or 0 for the scenarios without recurrent inhibition. The inhibitory post-synaptic potential amplitude was gradually reduced for motor neurons of increasing size, with the largest motor neuron in a given pool receiving inhibitory post-synaptic potentials at only 30% of their initial amplitude. This approach minimizes the number of silent motoneurons, and is consistent with reports suggesting that recurrent inhibition is biased towards slow, fatigue-resistant motoneurons (68). The synaptic delay in either direction (from motoneurons to Renshaw cells and from Renshaw cells to motoneurons) was set to 1 ms (35).

4.5.3. Input to the simulated neurons

The simulated motor neurons received a mixture of inputs in the proportions proposed by Farina & Negro (69): 37% common excitatory inputs (0-5 Hz bandwidth), 13% common noise (0-10 Hz bandwidth), and 50% independent noise (0-50 Hz bandwidth) (Fig. 4.A). These signals had a mean of 0 and standard deviation of 0.15, and they were added to a baseline excitatory input of 1.6 (simulations without recurrent inhibition) or 1.7 (simulations with recurrent inhibition). The baseline excitation was increased in the presence of recurrent inhibition to maintain similar average firing rates of the motor neurons across the simulation scenarios. Each simulated Renshaw cell received an independent input with a mean of 0.3, and a standard deviation of 0.3. For simulations with recurrent inhibition, all of the motor neurons within a given pool received the same common input. These inputs consisted of the z-transformed cumulative spike trains of subsamples of VL motor units recorded during the reference contractions of the first experiment (see above) convolved with a 200-ms Hanning window with no phase shift. The resulting three input signals were well correlated (r=0.70 ±0.11), but not identical, which is consistent with reports of a high proportion of common inputs shared between the Vastii (19, 38). In the simulation scenario with multiple common inputs and without recurrent inhibition, the three common inputs were heterogeneously distributed among the motor neurons of a given pool, with the same three common inputs used for all pools. These three common inputs were the z-transformed first three principal components of the smoothed firing rates recorded from the VL during the reference contraction

in the first experiment. The common and independent noises were low-pass-filtered Gaussian noise with a cutoff frequencies of 10 and 50 Hz, respectively. All the motor neurons within a given pool received the same common noise, and each motor neuron received different independent noise.

4.5.4. Simulation parameters and analysis of simulated data

Seven simulations were performed for each of the four scenarios (the "control scenario", the "multiple common inputs scenario", the "homonymous recurrent inhibition scenario", and the "homonymous and heteronymous recurrent inhibition scenario" – as described in the Results section), with each simulation using common input(s) derived from experimental data of a different participant, with timesteps of 0.1 ms (total duration of 20 s). The input values, as well as the excitatory post-synaptic potentials of motor neurons and the inhibitory post-synaptic potentials of Renshaw cells, were manually tuned to achieve physiologically plausible neuronal activity, resulting in a mean firing rate of motor neurons and Renshaw cells within the 8-10 Hz range. We preprocessed and analyzed the simulated spike trains of the alpha motor neurons innervating the VL muscle in the same manner as the experimentally recorded spike trains (see above).

4. 5. Statistical analysis

All statistical analyses were conducted using the R software (R Development Core Team, 2023). The significance threshold was set to 0.05 and adjusted using the Bonferroni correction for multiple tests. Logistic regression models were used to compare the *dispersion* and *displacement* values (dependent variables) between the muscles and contraction types (predictors), with one model per dependent variable. In all models, 'Muscle' (GM-GM; VL-VL), 'Contraction type' (sinusoidal 0.25 Hz; sinusoidal 1 Hz; sinusoidal 3 Hz) and the interaction between 'Muscle' and 'Contraction type' were specified as fixed factors. For each dependent variable, we compared three different model structures with random effects of increasing complexity: no random effects, one intercept per participant, and one intercept per contraction type per participant. Notably, we did not use the 'Muscle' factor in the random effect because the VL and GM experiments involved different participants. In all cases, using one intercept per contraction type per participant as a random effect resulted in the lowest Akaike information criterion and Bayesian information criterion values ($p<0.001$). The selected models thus had the following structure: *"model <= lmer(dependent_variable*

*[dispersion or displacement] ~ muscle * contraction_type + (contraction_type | participant)".* The statistical significance of the fixed factors were tested using the "anova()" function. Post-hoc pairwise comparisons consisted of contrasting estimated marginal means against each other with Bonferroni-adjusted repeated t-tests. These comparisons were performed using the "emmeans()" function (emmeans package). When testing for the effect of contraction types conditioning on muscles, a repeated-measures design was considered.

5. References

1. C. J. de Luca, R. S. LeFever, M. P. McCue, A. P. Xenakis, Control scheme governing concurrently active human motor units during voluntary contractions. *The Journal of Physiology* **329**, 129–142 (1982).

2. F. Negro, A. Holobar, D. Farina, Fluctuations in isometric muscle force can be described by one linear projection of low-frequency components of motor unit discharge rates. *The Journal of Physiology* **587**, 5925–5938 (2009).

3. A. Schmied, J. P. Vedel, S. Pagni, Human spinal lateralization assessed from motoneurone synchronization: dependence on handedness and motor unit type. *The Journal of Physiology* **480**, 369–387 (1994).

4. E. Henneman, Relation between Size of Neurons and Their Susceptibility to Discharge. *Science* **126**, 1345–1347 (1957).

5. J. E. Desmedt, E. Godaux, Spinal motoneuron recruitment in man: rank deordering with direction but not with speed of voluntary movement. *Science* **214**, 933–936 (1981).

6. B. M. Ter Haar Romeny, J. J. D. Van Der Gon, C. C. A. M. Gielen, Changes in recruitment order of motor units in the human biceps muscle. *Experimental Neurology* **78**, 360–368 (1982).

7. U. Herrmann, M. Flanders, Directional Tuning of Single Motor Units. *J. Neurosci.* **18**, 8402–8416 (1998).

8. N. J. Marshall, *et al.*, Flexible neural control of motor units. *Nat Neurosci* (2022). https://doi.org/10.1038/s41593-022-01165-8.

9. E. Formento, P. Botros, J. M. Carmena, Skilled independent control of individual motor units via a non-invasive neuromuscular–machine interface. *J. Neural Eng.* **18**, 066019 (2021).

10. P. N. S. Bawa, K. E. Jones, R. B. Stein, Assessment of size ordered recruitment. *Front. Hum. Neurosci.* **8** (2014).

11. F. Hug, S. Avrillon, J. Ibáñez, D. Farina, Common synaptic input, synergies and size principle: Control of spinal motor neurons for movement generation. *The Journal of Physiology* **601**, 11–20 (2023).

12. A. Del Vecchio, *et al.*, The Forces Generated by Agonist Muscles during Isometric Contractions Arise from Motor Unit Synergies. *J. Neurosci.* **43**, 2860–2873 (2023).

13. S. Madarshahian, M. L. Latash, Synergies at the level of motor units in single-finger and multi-finger tasks. *Exp Brain Res* **239**, 2905–2923 (2021).

14. J. M. Ricotta, *et al.*, Motor unit-based synergies in a non-compartmentalized muscle. *Exp Brain Res* **241**, 1367–1379 (2023).

15. M. Bräcklein, *et al.*, The control and training of single motor units in isometric tasks are constrained by a common input signal. *eLife* **11**, e72871 (2022).

16. D. Adam, U. Windhorst, G. F. Inbar, The effects of recurrent inhibition on the cross-correlated firing patterns of motoneurones (and their relation to signal transmission in the spinal cord-muscle channel). *Biol. Cybernetics* **29**, 229–235 (1978).

17. J. C. Eccles, R. M. Eccles, A. Iggo, M. Ito, Distribution of recurrent inhibition among motoneurones. *The Journal of Physiology* **159**, 479–499 (1961).

18. M. G. Maltenfort, C. J. Heckman, W. Z. Rymer, Decorrelating Actions of Renshaw Interneurons on the Firing of Spinal Motoneurons Within a Motor Nucleus: A Simulation Study. *Journal of Neurophysiology* **80**, 309–323 (1998).

19. S. Avrillon, *et al.*, Individual differences in the neural strategies to control the lateral and medial head of the quadriceps during a mechanically constrained task. *Journal of Applied Physiology* **130**, 269–281 (2021).

20. F. Hug, A. Del Vecchio, S. Avrillon, D. Farina, K. Tucker, Muscles from the same muscle group do not necessarily share common drive: evidence from the human triceps surae. *Journal of Applied Physiology* **130**, 342–354 (2021).

21. S. A. Edgley, E. R. Williams, S. N. Baker, Spatial and Temporal Arrangement of Recurrent Inhibition in the Primate Upper Limb. *J. Neurosci.* **41**, 1443–1454 (2021).

22. M. L. McCurdy, T. M. Hamm, Recurrent collaterals of motoneurons projecting to distal muscles in the cat hindlimb. *Journal of Neurophysiology* **67**, 1359–1366 (1992).

23. A. Holobar, D. Zazula, Multichannel Blind Source Separation Using Convolution Kernel Compensation. *IEEE Transactions on Signal Processing* **55**, 4487–4496 (2007).

24. A. H. Caillet, *et al.*, Larger and Denser: An Optimal Design for Surface Grids of EMG Electrodes to Identify Greater and More Representative Samples of Motor Units. *eNeuro* **10** (2023).

25. J. P. Cunningham, B. M. Yu, Dimensionality reduction for large-scale neural recordings. *Nat Neurosci* **17**, 1500–1509 (2014).

26. B. DePasquale, D. Sussillo, L. F. Abbott, M. M. Churchland, The centrality of population-level factors to network computation is demonstrated by a versatile approach for training spiking networks. *Neuron* **111**, 631-649.e10 (2023).

27. J. A. Gallego, M. G. Perich, L. E. Miller, S. A. Solla, Neural Manifolds for the Control of Movement. *Neuron* **94**, 978–984 (2017).

28. K. V. Shenoy, M. Sahani, M. M. Churchland, Cortical Control of Arm Movements: A Dynamical Systems Perspective. *Annu. Rev. Neurosci.* **36**, 337–359 (2013).

29. V. C. K. Cheung, *et al.*, Stability of muscle synergies for voluntary actions after cortical stroke in humans. *Proceedings of the National Academy of Sciences* **106**, 19563–19568 (2009).

30. V. C. K. Cheung, A. d'Avella, M. C. Tresch, E. Bizzi, Central and Sensory Contributions to the Activation and Organization of Muscle Synergies during Natural Motor Behaviors. *J. Neurosci.* **25**, 6419–6434 (2005).

31. D. J. Clark, L. H. Ting, F. E. Zajac, R. R. Neptune, S. A. Kautz, Merging of Healthy Motor Modules Predicts Reduced Locomotor Performance and Muscle Coordination Complexity Post-Stroke. *Journal of Neurophysiology* **103**, 844–857 (2010).

32. J. Levine, S. Avrillon, D. Farina, F. Hug, J. L. Pons, Two motor neuron synergies, invariant across ankle joint angles, activate the triceps surae during plantarflexion. *The Journal of Physiology* JP284503 (2023).

33. F. Hug, P. W. Hodges, K. Tucker, Task dependency of motor adaptations to an acute noxious stimulation. *Journal of Neurophysiology* **111**, 2298–2306 (2014).

34. A. Bernacchia, X.-J. Wang, Decorrelation by Recurrent Inhibition in Heterogeneous Neural Circuits. *Neural Computation* **25**, 1732–1767 (2013).

35. E. R. Williams, S. N. Baker, Renshaw Cell Recurrent Inhibition Improves Physiological Tremor by Reducing Corticomuscular Coupling at 10 Hz. *J. Neurosci.* **29**, 6616–6624 (2009).

36. R. M. Brownstone, T. V. Bui, "Spinal interneurons providing input to the final common path during locomotion" in *Progress in Brain Research*, (Elsevier, 2010), pp. 81–95.

37. M. L. McCurdy, T. M. Hamm, Topography of recurrent inhibitory postsynaptic potentials between individual motoneurons in the cat. *Journal of Neurophysiology* **72**, 214–226 (1994).

38. C. M. Laine, E. Martinez-Valdes, D. Falla, F. Mayer, D. Farina, Motor Neuron Pools of Synergistic Thigh Muscles Share Most of Their Synaptic Input. *Journal of Neuroscience* **35**, 12207–12216 (2015).

39. D. Farina, F. Negro, J. L. Dideriksen, The effective neural drive to muscles is the common synaptic input to motor neurons. *J Physiol* **592**, 3427–3441 (2014).

40. D. A. Keen, A. J. Fuglevand, Distribution of Motor Unit Force in Human Extensor Digitorum Assessed By Spike-Triggered Averaging and Intraneural Microstimulation. *Journal of Neurophysiology* **91**, 2515–2523 (2004).

41. T. L. McIsaac, A. J. Fuglevand, Motor-Unit Synchrony Within and Across Compartments of the Human Flexor Digitorum Superficialis. *Journal of Neurophysiology* **97**, 550–556 (2007).

42. K. T. Reilly, M. A. Nordstrom, M. H. Schieber, Short-Term Synchronization Between Motor Units in Different Functional Subdivisions of the Human Flexor Digitorum Profundus Muscle. *Journal of Neurophysiology* **92**, 734–742 (2004).

43. L. Grimby, J. Hannerz, Firing rate and recruitment order of toe extensor motor units in different modes of voluntary conraction. *The Journal of Physiology* **264**, 865–879 (1977).

44. J. Rossato, S. Avrillon, K. Tucker, D. Farina, F. Hug, The volitional control of individual motor units is constrained within low-dimensional neural manifolds by common inputs. *J. Neurosci.* e0702242024 (2024).

45. C. J. Heckman, R. M. Enoka, "Motor Unit" in *Comprehensive Physiology*, 1st Ed., R. Terjung, Ed. (Wiley, 2012), pp. 2629–2682.

46. F. Baldissera, H. Hultborn, M. Illert, "Integration in Spinal Neuronal Systems" in *Comprehensive Physiology*, 1st Ed., R. Terjung, Ed. (Wiley, 1981), pp. 509–595.

47. C. J. De Luca, Z. Erim, Common Drive in Motor Units of a Synergistic Muscle Pair. *Journal of Neurophysiology* **87**, 2200–2204 (2002).

48. R. Katz, E. Pierrot-Deseilligny, Recurrent inhibition in humans. *Progress in Neurobiology* **57**, 325–355 (1999).

49. S. Cullheim, J. O. Kellerth, A morphological study of the axons and recurrent axon collaterals of cat alpha-motoneurones supplying different hind-limb muscles. *The Journal of Physiology* **281**, 285–299 (1978).

50. A. Rossi, R. Mazzocchio, Presence of homonymous recurrent inhibition in motoneurones supplying different lower limb muscles in humans. *Exp Brain Res* **84** (1991).

51. U. Windhorst, THE SPINAL CORD AND ITS BRAIN: REPRESENTATIONS AND MODELS. TO WHAT EXTENT DO FOREBRAIN MECHANISMS APPEAR AT BRAINSTEM SPINAL CORD LEVELS? *Progress in Neurobiology* **49**, 381–414 (1996).

52. D. A. Keen, L.-W. Chou, M. A. Nordstrom, A. J. Fuglevand, Short-term synchrony in diverse motor nuclei presumed to receive different extents of direct cortical input. *Journal of Neurophysiology* **108**, 3264–3275 (2012).

53. F. Negro, U. Ş. Yavuz, D. Farina, The human motor neuron pools receive a dominant slow-varying common synaptic input. *The Journal of Physiology* **594**, 5491–5505 (2016).

54. C. Alessandro, *et al.*, Coordination amongst quadriceps muscles suggests neural regulation of internal joint stresses, not simplification of task performance. *Proc. Natl. Acad. Sci. U.S.A.* **117**, 8135–8142 (2020).

55. T. V. Trank, V. V. Turkin, T. M. Hamm, Organization of recurrent inhibition and facilitation in motoneuron pools innervating dorsiflexors of the cat hindlimb. *Experimental Brain Research* **125**, 344–352 (1999).

56. G. R. Chalmers, P. Bawa, Synaptic connections from large afferents of wrist flexor and extensor muscles to synergistic motoneurones in man: *Exp Brain Res* **116**, 351–358 (1997).

57. J. Rossato, *et al.*, I-Spin live: An open-source software based on blind-source separation for decoding the activity of spinal alpha motor neurons in real-time. [Preprint] (2023). Available at: https://elifesciences.org/reviewed-preprints/88670v1 [Accessed 20 July 2024].

58. F. Negro, S. Muceli, A. M. Castronovo, A. Holobar, D. Farina, Multi-channel intramuscular and surface EMG decomposition by convolutive blind source separation. *J. Neural Eng.* **13**, 026027 (2016).

59. S. Avrillon, F. Hug, S. N. Baker, C. Gibbs, D. Farina, Tutorial on MUedit: An open-source software for identifying and analysing the discharge timing of motor units from electromyographic signals. *Journal of Electromyography and Kinesiology* **77**, 102886 (2024).

60. A. Del Vecchio, *et al.*, Tutorial: Analysis of motor unit discharge characteristics from high-density surface EMG signals. *Journal of Electromyography and Kinesiology* **53**, 102426 (2020).

61. F. Hug, *et al.*, Analysis of motor unit spike trains estimated from high-density surface electromyography is highly reliable across operators. *Journal of Electromyography and Kinesiology* **58**, 102548 (2021).

62. A. Holobar, M. A. Minetto, A. Botter, F. Negro, D. Farina, Experimental Analysis of Accuracy in the Identification of Motor Unit Spike Trains From High-Density Surface EMG. *IEEE Trans. Neural Syst. Rehabil. Eng.* **18**, 221–229 (2010).

63. A. Frančič, A. Holobar, "On the Reuse of Motor Unit Filters in High Density Surface Electromyograms with Different Signal-to-Noise Ratios" in *8th European Medical and Biological Engineering Conference*, IFMBE Proceedings., T. Jarm, A. Cvetkoska, S. Mahnič-Kalamiza, D. Miklavcic, Eds. (Springer International Publishing, 2021), pp. 923–931.

64. M. Stimberg, R. Brette, D. F. Goodman, Brian 2, an intuitive and efficient neural simulator. *eLife* **8**, e47314 (2019).

65. A. H. Caillet, A. T. Phillips, D. Farina, L. Modenese, Mathematical relationships between spinal motoneuron properties. *eLife* **11**, e76489 (2022).

66. M. Manuel, M. Chardon, V. Tysseling, C. J. Heckman, Scaling of Motor Output, From Mouse to Humans. *Physiology* **34**, 5–13 (2019).

67. J. Borg, Effects of prior activity on the conduction in single motor units in man. *Journal of Neurology, Neurosurgery & Psychiatry* **46**, 317–321 (1983).

68. W. A. Friedman, G. W. Sypert, J. B. Munson, J. W. Fleshman, Recurrent inhibition in type-identified motoneurons. *Journal of Neurophysiology* **46**, 1349–1359 (1981).

69. D. Farina, F. Negro, Common Synaptic Input to Motor Neurons, Motor Unit Synchronization, and Force Control. *Exercise and Sport Sciences Reviews* **43**, 23–33 (2015).

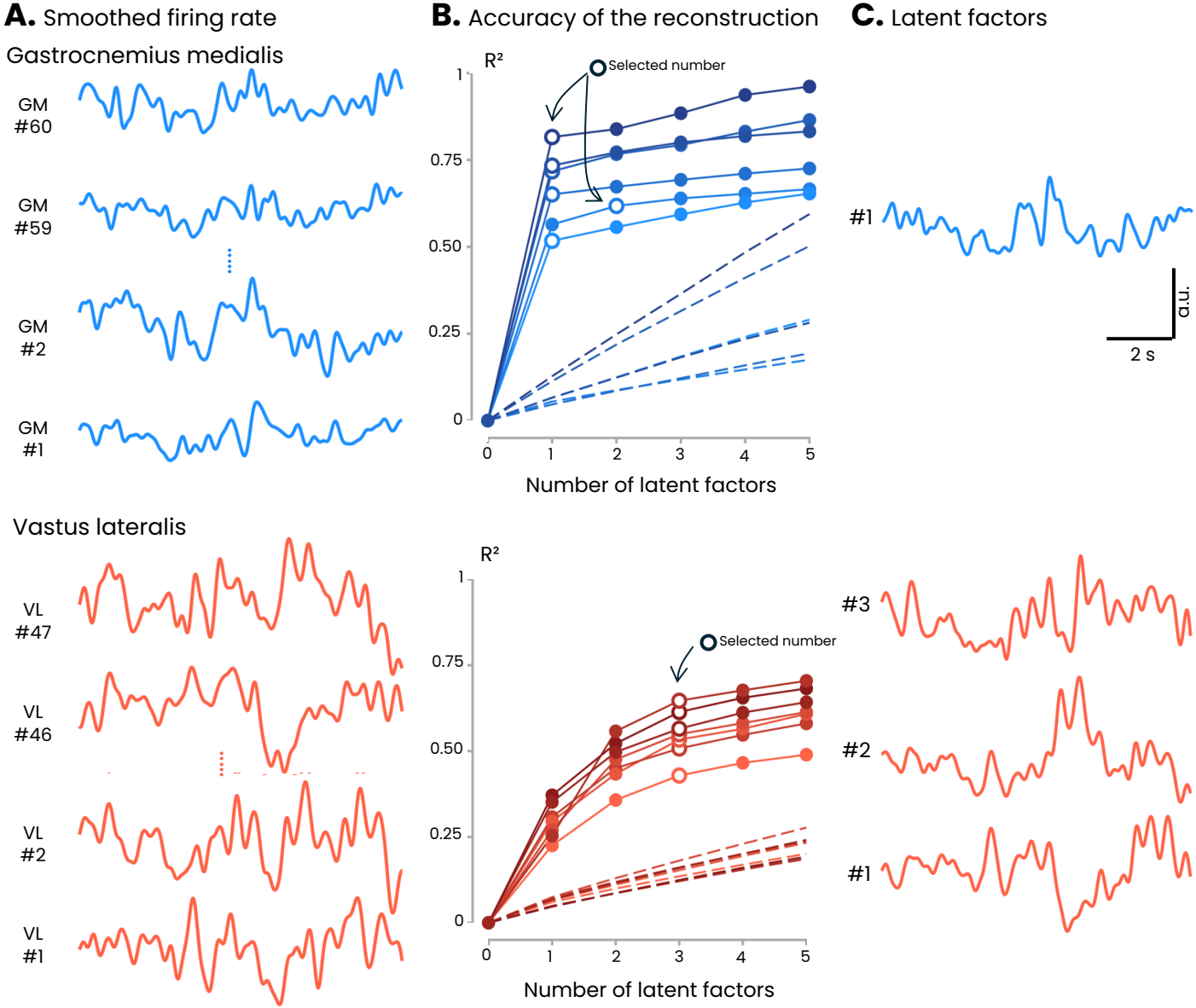
A. Smoothed firing rate
Gastrocnemius medialis
GM #60
GM #59
GM #2
GM #1
B. Accuracy of the reconstruction
R²
Selected number
1
0.75
0.50
0.25
0
0
1
2
3
4
5
Number of latent factors
C. Latent factors
#1
a.u.
2 s
Vastus lateralis
VL #47
VL #46
VL #2
VL #1
R²
Selected number
1
0.75
0.50
0.25
0
0
1
2
3
4
5
Number of latent factors
#3
#2
#1

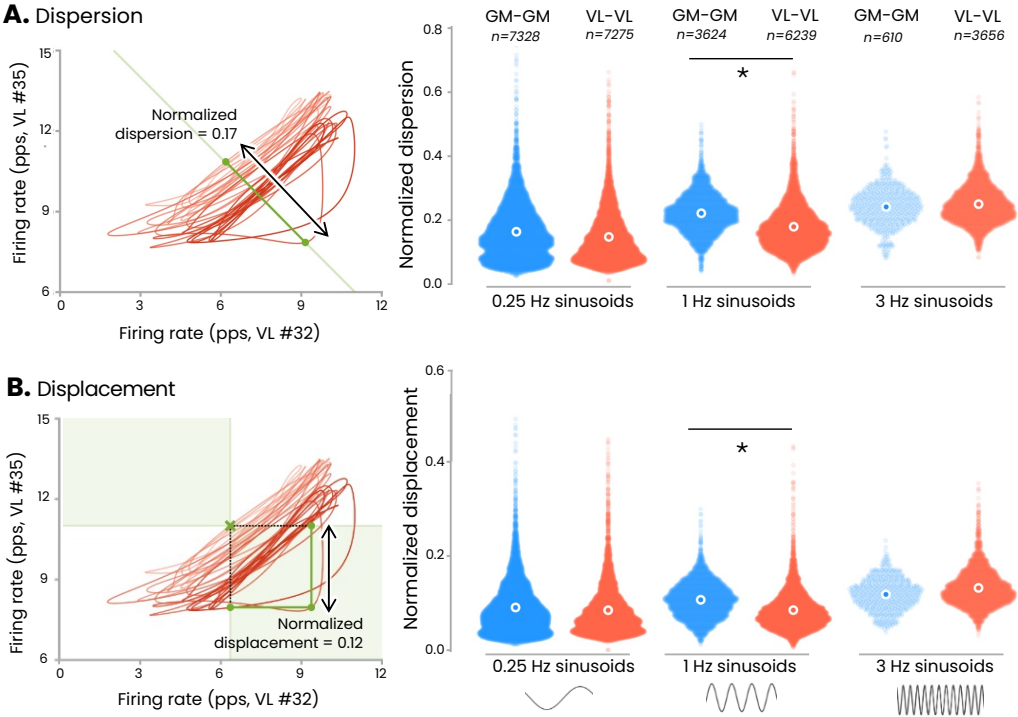
A. Dispersion
Normalized dispersion = 0.17
Firing rate (pps, VL #35)
Firing rate (pps, VL #32)
GM-GM n=7328
VL-VL n=7275
GM-GM n=3624
VL-VL n=6239
GM-GM n=610
VL-VL n=3656
Normalized dispersion
0.25 Hz sinusoids
1 Hz sinusoids
3 Hz sinusoids
B. Displacement
Normalized displacement = 0.12
Normalized displacement

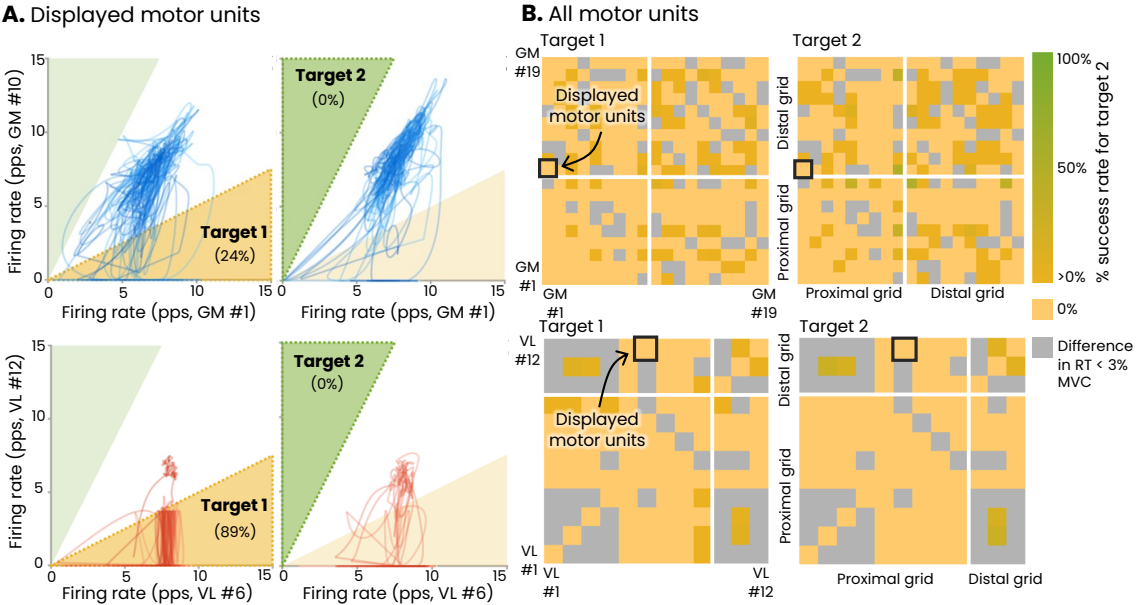
A. Displayed motor units
B. All motor units
Target 1
(24%)
Target 2
(0%)
Target 1
(89%)
Target 2
(0%)
Firing rate (pps, GM #10)
Firing rate (pps, GM #1)
Firing rate (pps, VL #12)
Firing rate (pps, VL #6)
Target 1
Target 2
Displayed motor units
GM #19
GM #1
VL #12
VL #1
Distal grid
Proximal grid
100%
50%
>0%
0%
% success rate for target 2
Difference in RT < 3% MVC

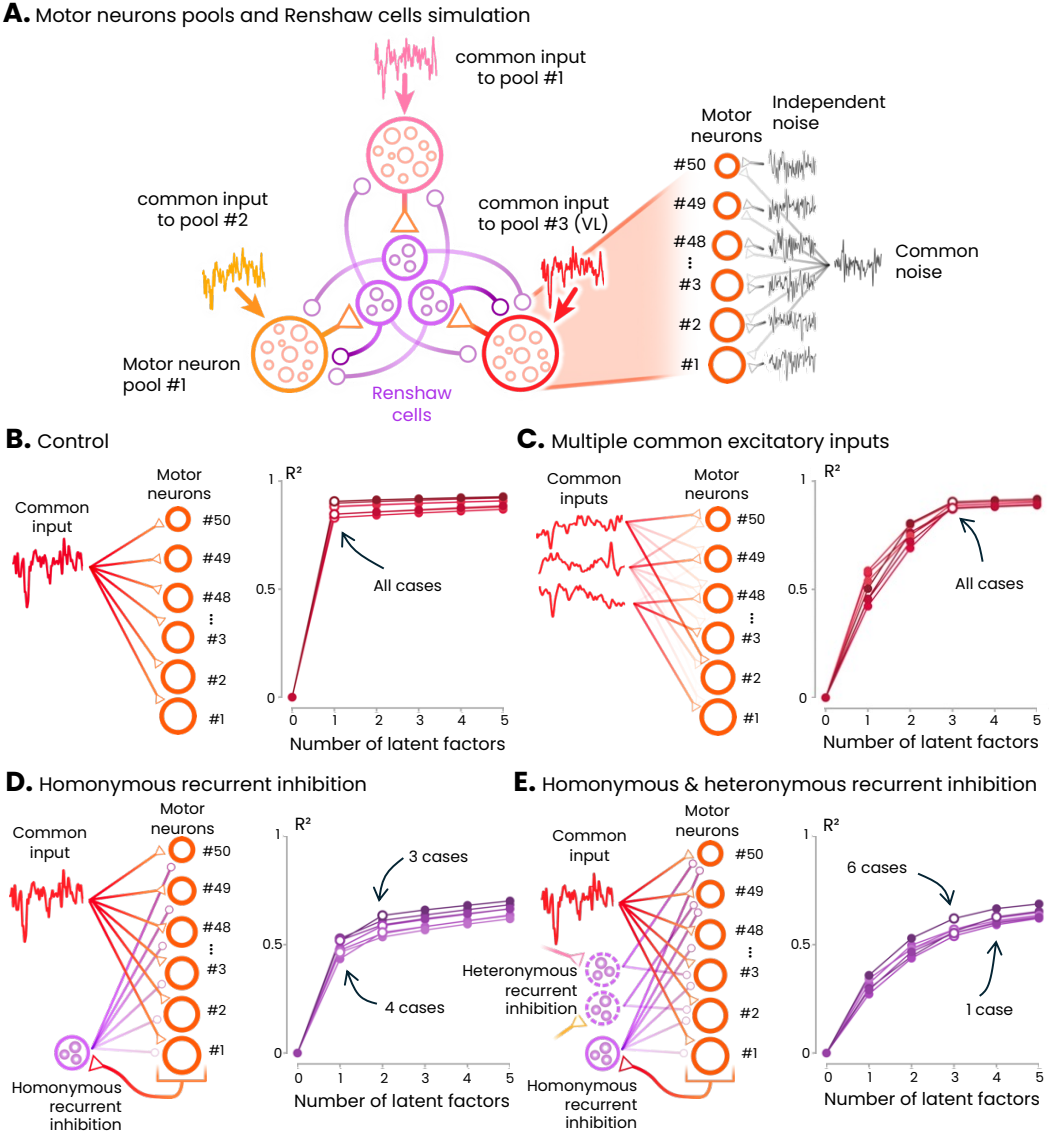
A. Motor neurons pools and Renshaw cells simulation
common input to pool #1
common input to pool #2
common input to pool #3 (VL)
Motor neuron pool #1
Renshaw cells
Motor neurons
Independent noise
Common noise
#50
#49
#48
#3
#2
#1
B. Control
Common input
Motor neurons
R²
All cases
Number of latent factors
C. Multiple common excitatory inputs
Common inputs
D. Homonymous recurrent inhibition
3 cases
4 cases
Homonymous recurrent inhibition
E. Homonymous & heteronymous recurrent inhibition
6 cases
1 case
Heteronymous recurrent inhibition